PHYSICAL REVIEW B

CONDENSED MATTER

THIRD SERIES, VOLUME 41, NUMBER 7 1 MARCH 1990

Fourier-transform and continuous-wave EPR studies of nickel in synthetic diamond: Site and spin multiplicity

J. Isoya
University of Library and Information Science, Kasuga 1-2, Tsukuba-city, Ibaraki-ken 305, Japan

H. Kanda
National Institute for Research in Inorganic Materials, 1-1 Namiki, Tsukuba-city, Ibaraki-ken 305, Japan

J. R. Norris, J. Tang, and M. K. Bowman
Chemistry Division, Argonne National Laboratory, Argonne, Illinois 60439
(Received 19 June 1989)

Pulsed, Fourier-transform, and continuous-wave electron paramagnetic resonance methods are used to study the $g=2.0319$ EPR signal in synthetic diamond crystals. This signal is from Ni which is found to be located at a substitutional site in the diamond lattice without detectable nearby charge compensation. The effective spin state of $S=\frac{3}{2}$ is determined from Fourier-transform nutational EPR spectroscopy. It is proposed that the center is a Ni^- ion with electronic configuration $3d^7$.

I. INTRODUCTION

The synthesis of large diamond crystals with dimensions exceeding 1.0 cm is now possible with recent developments in techniques and in apparatus for growing single crystals at high temperatures and pressures. The possibilities have opened up for the use of the unique properties of synthetic diamond single crystals in electronic devices,[1] since silicon lies directly below carbon on the Periodic Table and has crystals isostructural with diamond (bond length: C—C 1.54 Å, Si—Si 2.35 Å). Transition metals of the 3*d* group, Ti, V, Cr, Mn, Fe, and Ni are easily doped into silicon, introducing deep-acceptor or deep-donor levels.[2,3] These metal ions diffuse easily into silicon near its melting point. In diamond, however, nickel seems to be the only transition-metal ion which gives a well-established electron paramagnetic resonance (EPR) signal from dispersed impurities. This is true even of synthetic diamonds which are grown from a molten metal solvent typically containing Fe, Ni, Co, and Mn. Loubser and van Rynevald[4] found an EPR line with a *g* value of 2.0310 ± 0.0005 in synthetic polycrystalline diamond grown from a metal melt containing Ni. Since the signal was absent in samples grown from a melt without Ni, it was assigned to Ni. The assignment was confirmed by Samoilovich *et al.*,[5] who observed a 0.65 ± 0.05 mT hyperfine splitting from ^{61}Ni ($I=\frac{3}{2}$, natural abundance 1.2%) in isotopically enriched (86%) powdered samples.

The Ni EPR signal remains isotropic at temperatures as low as 4 K,[4,5] suggesting that it occupies a high-symmetry site and is not associated with a nearby impurity or vacancy. It has not been established whether the Ni occupies a substitutional or an interstitial site in the diamond crystals. In silicon, Ni is present as Ni^+ (electronic configuration $3d^9$, $S=\frac{1}{2}$), occupying an interstitial site[2] while in germanium, it is proposed that Ni^- ($3d^8$ with a bound hole in the valence shell, $S=\frac{1}{2}$) is present in a substitutional site.[6] In both silicon and germanium, the Ni spin state can be verified from the absence of fine structure in the anisotropic EPR spectra from distorted configurations observed at low temperatures. At higher temperatures, reorientation among the distorted configurations is sufficiently rapid to produce an isotropic EPR spectrum.

In single-crystal diamond, it has not been possible to determine by conventional cw-EPR measurements either the location or the effective spin of the Ni impurity since only isotropic EPR spectra are observed. Tetrahedral sites (either substitutional or interstitial) have sufficiently high symmetry that no fine structure is expected for all spin states with $S\leq\frac{3}{2}$. However, pulsed or Fourier-transform (FT) EPR has made it possible to measure the effective spin of the Ni impurity and determine its location within the diamond crystal.

II. EXPERIMENT

Four synthetic diamond crystals were used for this study. Three crystals, denoted *A*, *B*, and *C* were grown

 ©1990 The American Physical Society

in ~16 h at 6 GPa and 1700 K by the temperature gradient method.[7,8] Sample *A* (9 mg, green, [N]=1 ppm, [Ni]=0.4 ppm) was grown from an alloy of Ni with 2 wt. % Ti, using a powdered mixture of diamonds and graphite as the carbon source. The carbon source was wrapped in aluminum foil to decrease the nitrogen concentration in the crystal. Sample *B* (20 mg, green, [N]=2.8 ppm, [Ni]=0.8 ppm), 10% enriched in ^{13}C ($I=\frac{1}{2}$, natural abundance 1.1%) was prepared in the same manner as sample *A* except that the ^{13}C was supplied as amorphous carbon. Sample *C* (20 mg, yellow green, [N]=60 ppm, [Ni]=70 ppm) was grown from an alloy of Ni and Zr. The fourth crystal, sample *D* (45 mg, yellow, [N]=17 ppm, [Ni]=0.5 ppm), was supplied by Itami Laboratory, Sumitomo Electric Industries. The concentrations of Ni and N, denoted [Ni] and [N], respectively, were estimated from the EPR signal intensities for those impurities.

The FT-EPR measurements were made using spectrometers described previously[9-11] to measure the transients induced by 1 kW microwave pulses of about 9.2 GHz. Sample temperature was controlled using an Oxford Instruments ESR-900. The cw-EPR measurements were made using a Bruker ESP300 X-band spectrometer. The cw-EPR spectra were measured at 77 K using an insertion Dewar filled with liquid nitrogen and other temperatures were reached using a Bruker ER411VT variable temperature unit.

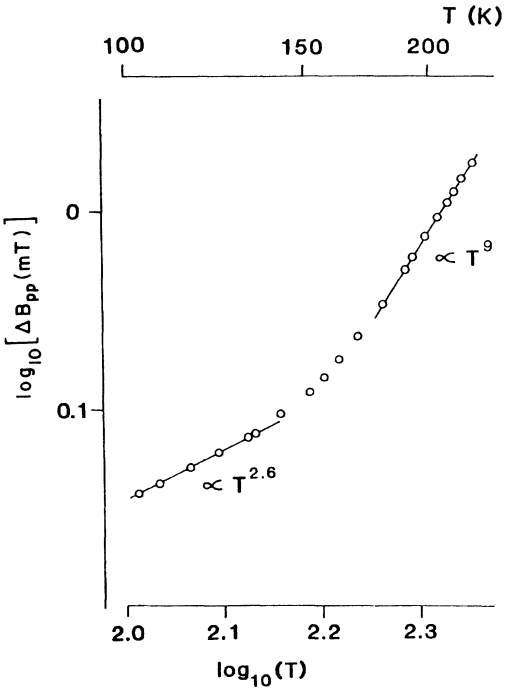

FIG. 1. Temperature dependence of the cw-EPR linewidth of the Ni impurity in synthetic diamond crystal *A* with the magnetic field $\mathbf{B}_0$ parallel to the [001] axis.

III. RESULTS AND DISCUSSION

A. Ni site

The EPR linewidth of the Ni impurity in diamond is very temperature dependent above 150 K. The spin-lattice relaxation of the Ni is responsible for the rapid increase of the cw-EPR linewidth from 0.10 mT at 150 K to 2.40 mT by 225 K, Fig. 1. However, at 77 K, the EPR linewidth is no longer determined by spin-lattice relaxation but rather by dipolar interactions with the paramagnetic impurities. In synthetic diamonds, the major paramagnetic impurities are dispersed nitrogens substituting for single carbon atoms in the lattice. The nitrogen impurity was first identified in natural diamonds.[12] At 77 K, the major contributions to the Ni EPR linewidth in most synthetic diamonds are dipole-dipole interactions between nitrogen and Ni and between Ni and Ni.[13] Sample *A*, with its low [Ni] and [N], has a peak-to-peak cw-EPR linewidth of only 0.025 mT at 77 K, allowing observation of not only the ^{61}Ni hyperfine lines in natural abundance but also the ^{13}C superhyperfine lines of the nearest-neighbor carbons in natural abundance, Fig. 2.

As the diamond crystal is rotated in the magnetic field of the EPR spectrometer, the center of the Ni spectrum does not vary and the ^{61}Ni hyperfine splitting does not change, $g=2.0319$ and $A(^{61}Ni)=0.65$ mT. On the other hand, the superhyperfine splittings from the nearest-neighbor ^{13}C do vary. A plot of the ^{13}C superhyperfine lines as the crystal is rotated about an axis perpendicular to the magnetic field, Fig. 3, is useful for identifying the local symmetry of the impurity site. In the diamond lattice, there are many sets of equivalent carbons around both the substitutional and the interstitial sites of tetrahedral symmetry. Each set of equivalent carbons can be classified as nearest neighbors, next-nearest neighbors, etc. based on the distance from the center of the site. Each set also belongs to one of four symmetry classes.[3,14,15] From the pattern of the rotational plots and the maximum number of observable lines, the symmetry class for each set of surrounding carbons can be assigned and the location of the tetrahedral site identified. This method has been applied for determination of impurity sites in silicon, usually using rotations about the [$\bar{1}$10] axis.[3,14,15]

The pattern in Fig. 3 shows three pairs of lines evenly split around the central Ni EPR line and connected by the solid curves. These EPR lines have relatively large anisotropy and are assigned to the nearest-neighbor carbons. The three sets of EPR lines have identical splittings along the [001] axis while only two of the splittings are identical along the [111] and [110] axes. The ^{13}C hyperfine tensor is axially symmetric around the [111] axis. These properties are characteristic of four carbons belonging to the 111 class. In this rotation, two carbons are magnetically equivalent and the pattern of the rotational plots consists of three sets of lines. Both the substitutional and the interstitial site are surrounded tetrahedrally by four nearest-neighbor, carbon atoms 1.54 Å distant. Each of the four carbons at the corners of the tetrahedron is on a threefold rotational symmetry axis

through the central ion and belongs to the 111 class. Thus the Ni must occupy a tetrahedral site although it is not possible to determine from the nearest-neighbor carbons whether that site is interstitial or substitutional. The ^{13}C hyperfine couplings for the nearest-neighbor carbons are given in Table I.

The substitutional site has 12 next-nearest neighbors 2.52 Å distant belonging to the 110 class while the interstitial site has only six next-nearest neighbors 1.78 Å distant belonging to the 100 class. Thus a definitive assignment of the Ni site can be made based on superhyperfine couplings of these next-nearest-neighbor carbons.

The cw-EPR spectra resolve at most only two sets of next-nearest-neighbor superhyperfine lines. The splitting is nearly isotropic (0.317 mT along the [001] axis, 0.374 and 0.290 mT along the [111] axis, 0.348 and 0.263 mT along the [110] axis), Fig. 3. Even with the EPR linewidth of 0.025 mT, it is not possible to resolve all three sets (interstitial site) or seven sets (substitutional site) of superhyperfine lines from the next-nearest neighbors. Conventional electron nuclear double resonance (ENDOR) has been used in similar cases to measure the hyperfine couplings from the ^{13}C directly. However, ENDOR is complicated in the present case by the possibility of cross relaxation (which is known to occur) between the Ni and the major paramagnetic center, nitrogen. It is possible for the ENDOR spectrum of the Ni to contain ^{13}C ENDOR lines of the nitrogen center. This potential problem is avoided entirely by the use of a FT-EPR technique we introduced in a study of ^{7}Li superhyperfine couplings with Ti^{3+} in α-quartz.[16] We use electron spin-nuclear spin coherences produced by an electron spin echo envelope modulation (ESEEM) experiment to measure the same couplings measured by ENDOR.[17–20] Superhyperfine couplings of the Ni are recorded by selectively detecting only those coherences involving the electron spin of the Ni.[16] A three-pulse, time-domain signal from the ^{13}C coupled with Ni in sample *B* is shown in Fig. 4.

The Fourier transform of this time-domain spectrum yields a frequency-domain spectrum containing the nuclear resonance frequencies for every set of ^{13}C coupled to the Ni. We are interested in the next-nearest neighbors of the Ni and initial analysis showed that all the necessary information needed to determine the Ni site

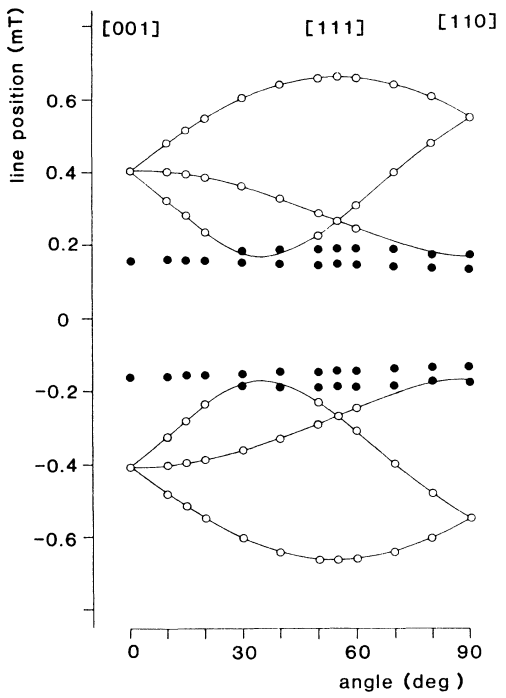

FIG. 3. Rotational dependence of the ^{13}C splittings of the nearest-neighbor carbons for the Ni impurity in synthetic diamond sample *A* at 77 K. The line positions of the ^{13}C superhyperfine lines are shown relative to that of the main line. The line positions of the partially resolved ^{13}C superhyperfine lines of the next-nearest-neighbor carbons are also shown in some orientations. The crystal was rotated with the magnetic field in the $(\bar{1}10)$ plane.

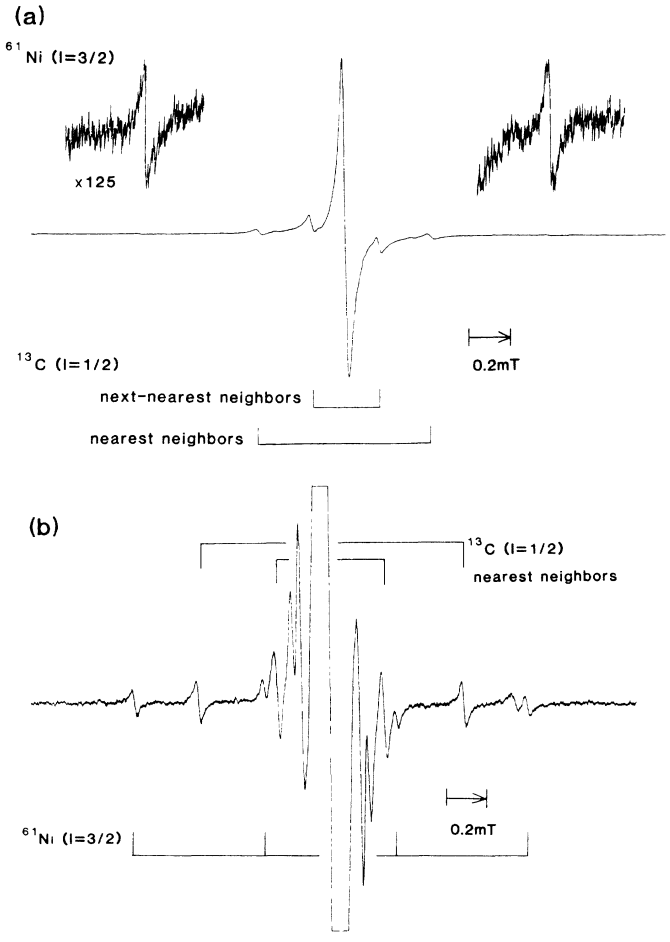

FIG. 2. cw-EPR spectra of the nickel center at 77 K in diamond sample *A* showing ^{61}Ni and ^{13}C lines in natural abundance. (a) **B** parallel to [001]. (b) **B** parallel to [111]. Spectra recorded with 100-KHz modulation and 0.01-mT modulation amplitude, with 0.2 mW at 9.533 GHz.

TABLE I. ^{13}C hyperfine couplings for the Ni impurity in synthetic diamond.

	$A_{\parallel}/g_0\mu_B$	$A_{\perp}/g_0\mu_B$	
Nearest neighbor	1.339 mT	0.340 mT	
	$A_1/g_0\mu_B$	$A_2/g_0\mu_B$	$A_3/g_0\mu_B$
Next-nearest neighbor	0.382 mT	0.272 mT	0.269 mT

lies between 7.0 and 9.0 MHz. Assuming a positive sign for the superhyperfine couplings since g_n of ^{13}C is positive, the modulation frequencies appearing in this region correspond to the ENDOR frequencies of the $m_s = -\frac{1}{2}$ level. We therefore used the LP-ZOOM linear-prediction method[21] to examine that region of the spectrum. The frequency-domain spectrum generated between 7.0 and 8.0 MHz, Fig. 5, contains two sharp lines at this orientation. The lines have a full width half height of about 20 kHz while the best cw-EPR spectra have a linewidth of 0.025 mT or 700 kHz. The better resolution in the FT-EPR experiment not only allows better resolution of the spectrum, but also allows accurate measurement of the small anisotropy of the next-nearest-neighbor couplings. The orientational dependences of the frequencies are plotted in Fig. 6. There are seven sets of frequencies observed. With the magnetic field parallel to the [001] axis, only two distinct frequencies are observed while along [111] only three are observed. These observations are expected for the next-nearest neighbors in a substitutional site (110 symmetry class) but not in an interstitial site (100 symmetry class). Thus Ni substitutes for carbon in the diamond lattice to produce the paramagnetic Ni center studied here.

The ^{13}C frequencies in Fig. 6 are consistent with the partially resolved, ^{13}C superhyperfine lines assigned to the next-nearest neighbors in Fig. 3. Each of the 12 carbons belonging to the 110 symmetry class is located in a (110) plane of reflection symmetry through the central ion. We shall describe the superhyperfine tensor using one assignable to the symmetry-related sites located in a $(\bar{1}10)$ plane through the central ion. One of the principal axes of the superhyperfine tensor lies along the $[\bar{1}10]$ axis and the other two are in the $(\bar{1}10)$ plane.[3,14,15] The principal axis with the largest principal value is 120° from the [001] axis in the $(\bar{1}10)$ plane. The principal values of the superhyperfine matrix were calculated from the angular dependence in Fig. 6 using the first-order equation $h\nu = |m_s A_{\text{eff}} - g_n \mu_n B|$ and are given in Table I. The principal value A_3 is associated with the principal axis along the $[\bar{1}10]$ axis.

The cw-EPR spectra of sample A recorded with the magnetic field parallel to the [001] axis has the superhyperfine lines from all four nearest neighbors superimposed by symmetry. At that orientation, only one set of lines is resolved for the next-nearest neighbors. The intensity of the superhyperfine lines from the next-nearest neighbors is 2.8 times the intensity from the nearest neighbors. Our measurements predict that at this orientation, the superhyperfine lines from the 12 next-nearest neighbors in a substitutional site will overlap, giving an intensity ratio of $\frac{12}{4}$ or 3 as observed. For an interstitial site, there are only six next-nearest neighbors, limiting the intensity ratio to $\frac{6}{4}$ or 1.5 at most. Thus the experimental intensity ratios agree with the substitutional model for Ni.

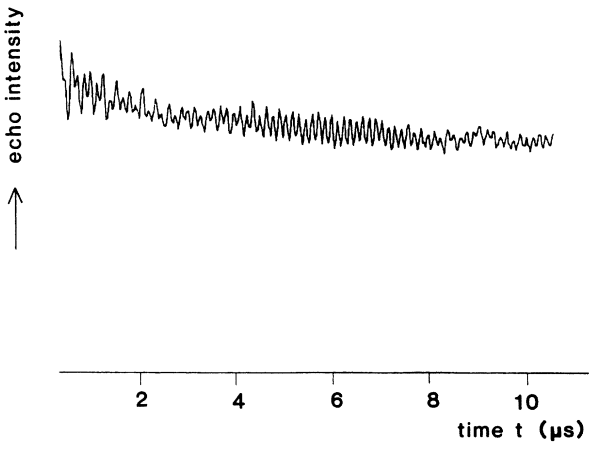

FIG. 4. Three-pulse echo modulation from the ^{13}C coupled to Ni in diamond sample B, doped with 10% ^{13}C. The magnetic field was parallel to the [111] axis at 45 K with the microwave frequency 9.2277 GHz, pulse power 200 W, and the spacing between the first and second pulses 0.40 μs. The spectrum consists of 512 points spaced 20 ns apart.

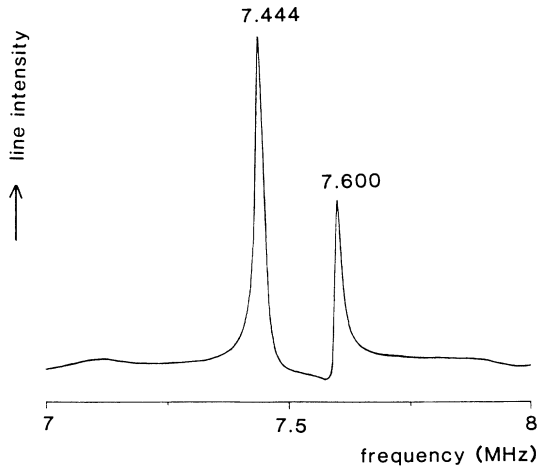

FIG. 5. A portion of the frequency-domain spectrum, obtained from the time-domain spectrum in Fig. 4, generated by LP-ZOOM showing two lines from ^{13}C coupled to Ni in diamond sample B (10% ^{13}C).

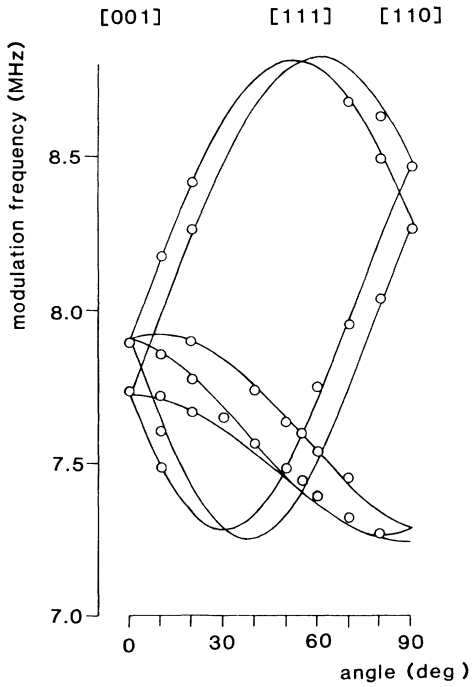

FIG. 6. Orientation dependence of the next-nearest-neighbor ^{13}C ENDOR frequencies of the $m_s=-\frac{1}{2}$ manifold as diamond sample B (10% ^{13}C) is rotated about the [$\bar{1}$10] axis at 45 K.

B. Ni spin

The effective, electron-spin state of the Ni is difficult to determine from cw-EPR spectra because the tetrahedral symmetry of the substitutional site makes the fine-structure splittings vanish for spin states with $S \leq \frac{3}{2}$. In principle, the spin state could be determined by careful analysis of the ^{13}C ESEEM frequencies measured above since they depend in part on the values of m_s. Unfortunately, a definitive theoretical analysis of ESEEM for $S > \frac{1}{2}$ has not been made for small or vanishing fine-structure splittings. The approach we use here is to measure $S_{\pm}$ from the nutation of the magnetization by the microwave magnetic field, B_1.

The free-induction decay (FID) following a single microwave pulse is proportional to $\sin(\omega_n t_p)$, where ω_n is the nutational frequency. If all EPR transitions for the spin are excited by the microwave pulse, then $\omega_n=\omega_1=\gamma B_1$. However, if B_1 is sufficiently small that only a single line in the spectrum is excited by the pulse, ω_n depends on the matrix element of $S_{\pm}$ operator for that transition. When only the $m_s=+\frac{1}{2}$ to $-\frac{1}{2}$ transition of a half-integral spin is excited, $\omega_n=(S+\frac{1}{2})\omega_1$ (Refs. 22 and 23) and if only one of the two transitions for an $S=1$ spin is excited, $\omega_n=2^{1/2}\omega_1$.

We recorded the nutational frequency for the Ni by monitoring the amplitude of the FT-EPR line as a function of the pulse duration t_p. The nitrogen center in diamond ($S=\frac{1}{2}$) at room temperature was used to calibrate ω_1. The amplitude of the FT-EPR signal from Ni in sample D at 77 K shows a clear sinusoidal pattern, Fig. 7(a), with $\omega_n/2\pi=\omega_1/2\pi\approx 16$ MHz. This measurement is not very indicative of spin state for the Ni since any center with $S\leq\frac{3}{2}$ in a perfect tetrahedral environment would give this result. However, when the sample temperature was decreased below 40 K, a second nutational frequency appears at $\omega_n=2\omega_1$, Fig. 7(b). The relative amount of the new component increases as the temperature decreases until at 25 K, it accounts for about 30% of the total signal. This new component has the same resonant frequency, g factor, and linewidth as the normal Ni signal and has the ω_n expected for an $S=\frac{3}{2}$ center in a site with lower symmetry than tetrahedral. This component has been observed in other samples at even higher temperatures.

We believe that at low temperature, Ni can adopt a slightly distorted configuration in the diamond lattice. The distortion is sufficient to produce fine-structure splittings larger than ω_1,[23] but small enough that the second-

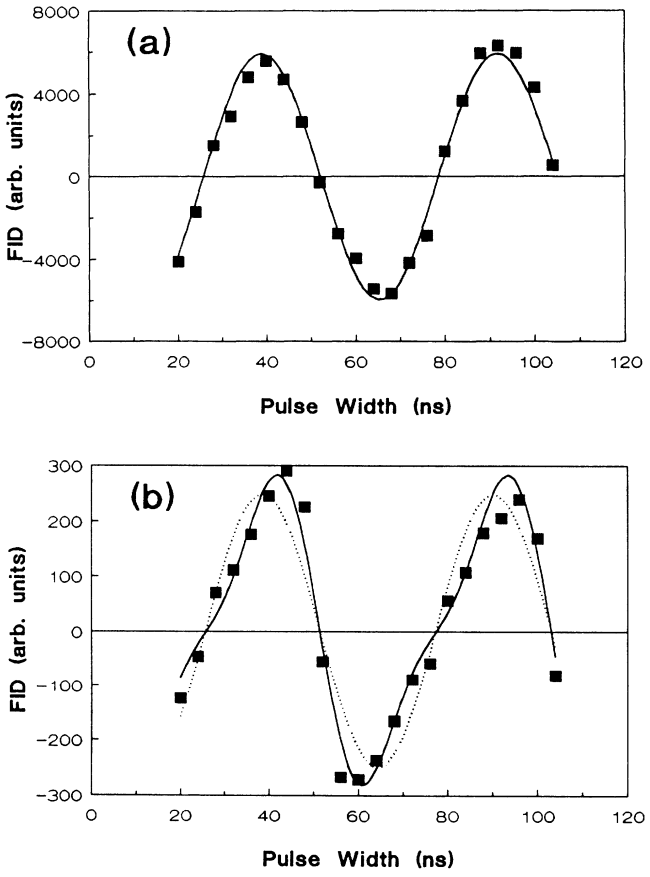

FIG. 7. Spin nutation of paramagnetic centers in synthetic diamond sample D. (a) The nickel center in sample D at 77 K. The solid line is fit to a single frequency at ω_1. (b) The Ni center at 25 K. The dashed line is a fit to a single frequency at ω_1, the solid line to frequencies at ω_1 and $2\omega_1$, showing the presence of the distorted form of an $S=\frac{3}{2}$ center.

order shifts on the $m_s = +\frac{1}{2}$ to $-\frac{1}{2}$ transition are less than the linewidth.[24] If the distortion is induced by random strains in the lattice or by distant, charge-compensating ions, the fine-structure splittings will have many different amplitudes and directions in the crystal and the other EPR transitions would be too broad to be detected.

We have previously measured local concentrations of nitrogen centers in synthetic diamonds[13] using instantaneous diffusion. The phenomenon of instantaneous diffusion relates spin relaxation rates to local dipolar fields (or concentrations) and the turning angle of the pulses, $\theta_p = \omega_n t_p$.[19,25,26] Here we invert that process and use the variation of spin relaxation rates with B_1 to measure ω_n in sample C. Figure 8 shows the results for measurements on nitrogen and Ni centers. The data from the nitrogen are used to experimentally measure the turning angle for $S = \frac{1}{2}$ and agree well with theory. The data from Ni at 48 K clearly do not fit the predictions for $S = \frac{1}{2}$. Instead, the Ni data are described well by the predictions based on $S = \frac{3}{2}$ for Ni with a mixture of distorted and undistorted sites. Thus the instantaneous diffusion measurements also indicate that Ni has $S = \frac{3}{2}$.

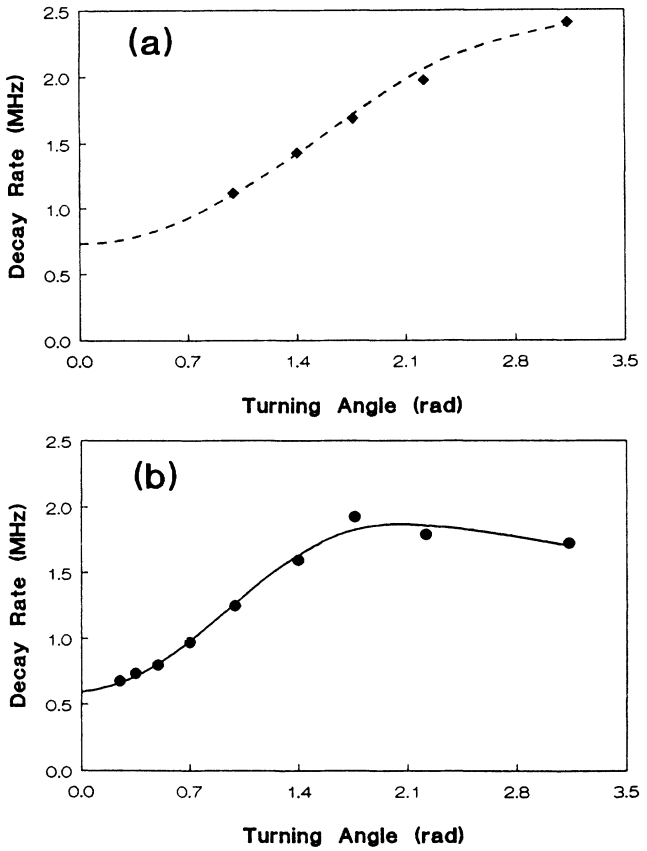

FIG. 8. Dependence of the phase memory relaxation rate on B_1 produced by instantaneous diffusion in diamond sample C. (a) Relaxation of the nitrogen center at room temperature produced by other nitrogen centers, $S = \frac{1}{2}$. The dashed line is a least-squares fit of the theoretical dependence to the data. (b) Relaxation of Ni centers at 48 K produced by Ni. The solid line is a least-squares fit including instantaneous diffusion from distorted and undistorted forms of Ni with $S = \frac{3}{2}$.

Further corroboration for the Ni spin comes from the ^{13}C nuclear frequencies measured above. Although the complete theory has not been worked out for $S = \frac{3}{2}$, it is reasonable to expect that the modulation includes most of the ENDOR frequencies. To first order, the ENDOR frequencies are $h\nu = |m_s A_{\text{eff}} - g_n \mu_n B|$ where A_{eff} are the hyperfine splittings. Using approximate values of A_{eff} measured from the cw-EPR spectra, the ENDOR frequencies can be estimated. With the magnetic field along the [001] axis, $|A_{\text{eff}}|$ for the next-nearest neighbors is 0.317 mT. To first order, the ENDOR frequency for the $m_s = -\frac{1}{2}$ manifold for either $S = \frac{1}{2}$ or $S = \frac{3}{2}$ is estimated to be 7.98 MHz assuming A_{eff} positive and $g_n = 1.4044$. The measured modulation frequencies, 7.74 and 7.89 MHz, at this orientation are consistent with this interpretation. The ENDOR frequencies calculated for $S = 1$ do not match any of the observed frequencies. Assuming that the 7.74- and 7.89-MHz frequencies belong to the $m_s = -\frac{1}{2}$ manifold of an $S = \frac{3}{2}$ ion, the ENDOR frequencies are estimated to be 9.34 and 9.79 MHz for the $m_s = +\frac{3}{2}$ manifold and 16.28 and 16.73 MHz for the $m_s = -\frac{3}{2}$ manifold. Weak lines are observed at 9.38, 9.77, 16.23, and 16.65 MHz. These frequencies are definitely inconsistent with an $S = \frac{1}{2}$ spin state for which the theory is well developed. Thus the modulation supports the assignment that $S = \frac{3}{2}$. The principal values of the superhyperfine matrix given in Table I were calculated using this assignment.

C. Ni electronic configuration

Transition-metal impurities in semiconductors form deep states in the energy gap and occur in several charge states. These semiconductor impurities have provided some classic examples of EPR spectra of transition-metal ions in a tetrahedral coordination environment. A simple model for explaining the EPR spectra of transition-metal impurities in silicon and germanium was presented by Ludwig and Woodbury.[2] Substitutional transition-metal ions in silicon and germanium transfer $3d$ electrons to the valence shell in order to complete tetrahedral bonds with the nearest neighbors. Thus transition-metal ions having a free-ion configuration of $3d^n 4s^2$ are expected to have an electronic configuration $3d^{n-2}$. In the substitutional site, the tetrahedral crystal field splits the $3d$ orbitals into the subsets e and t_2, with the e lower in energy. In the tetrahedral interstitial site in silicon and germanium, transition-metal ions having a free-ion configuration of $3d^n 4s^2$ show an electronic configuration $3d^{n+2}$, since the $4s$ electrons are transferred to the $3d$ shell. At the interstitial site, the $3d$ states also split into a triplet t_2 and a doublet e, however, the t_2 is lower in energy. It is likely that the octahedral crystal field from the next-nearest neighbors dominates the tetrahedral field from the nearest neighbors.

We assume that this simple model should be applicable to our case of nickel in diamond. With the effective spin

$S=\frac{3}{2}$ and with a g value close to that of the free electron, the nickel center in diamond is likely to be substitutional Ni^- with electronic configuration $3d^7$. The electronic ground state of a $3d^7$ ion in tetrahedral symmetry is an orbitally nondegenerate $^4A_2$ state ($e^4t_2^3$). With a non-orbitally-degenerate electronic configuration, the spin-lattice relaxation of Ni^- is expected to be slow and to allow easy EPR detection even at 77 K.

Nickel at the substitutional site of diamond should be observable by EPR if the charge state is either Ni^+ ($3d^5$, $S=\frac{5}{2}$), Ni^- ($3d^7$, $S=\frac{3}{2}$), or Ni^{3-} ($3d^9$, $S=\frac{1}{2}$). The determination of the spin multiplicity thus plays a critical role in determining the charge state. Nickel at the interstitial site in diamond should be easily observable by EPR if the charge state is either Ni^{2+} ($3d^8$, $S=1$) or Ni^+ ($3d^9$, $S=\frac{1}{2}$). At the interstitial site, an effective spin $S=\frac{3}{2}$ with an orbitally nondegenerate ground state requires an extremely high charge state of Ni^{7+} ($3d^3$), which is unlikely to occur. Thus the high spin multiplicity confirms our assignment of the nickel center to the substitutional site.

The EPR spectrum of a $3d^7$ ion with $S=\frac{3}{2}$ in tetrahedral symmetry is usually described by augmenting the conventional spin Hamiltonian with higher-order terms:[27]

$$u\mu_B\{S_x^3B_x+S_y^3B_y+S_z^3B_z-\tfrac{1}{5}(\mathbf{S}\cdot\mathbf{B})[3S(S+1)-1]\}\ , \tag{1}$$

where u is the amplitude of this term in the Hamiltonian. This term produces an anisotropy in the line position of the $m_s=+\frac{1}{2}$ to $-\frac{1}{2}$ transitions as well as producing fine structure. At 77 K, sample A exhibited a small degree of anisotropy in linewidth (0.025 mT along the [001] axis, 0.020 mT along the [111] axis, and 0.024 mT along the [110] axis), although the line position was isotropic within 0.008 mT. Since the nutation experiment shows that at 77 K, the three transitions of the $S=\frac{3}{2}$ spin are not split by a large amount, the coefficient of this high-order term must be very small.

D. Ni spin delocalization

We now consider the spin delocalization onto the nearest-neighbor carbons with a linear combination of atomic orbitals (LCAO) treatment which takes proper account of the symmetry and spin multiplicity. This treatment has been used for analysis of ENDOR data of interstitial transition-metal impurities in silicon.[3,28] In the simple crystal field approach, the three unpaired electrons in the substitutional Ni^- occupy the d_{xy}, d_{yz}, and d_{zx} orbitals. The t_2 states on the central ion have the proper symmetry to form σ bonds with the nearest-neighbor carbons, while the e states do not. Both the t_2 and e states may form π bonds with the nearest-neighbor carbons. By including covalency, these d_{xy}, d_{yz}, and d_{zx} orbitals are admixed with linear combinations of the $2s$ and $2p$ orbitals of surrounding carbons that transform as the t_2 irreducible representation of T_d symmetry. By neglecting the delocalization onto carbons further than the nearest neighbors and by neglecting the overlap between metal d orbitals and carbon orbitals, the wave functions of the unpaired electrons are[28]

$$\Psi_{xy}=\alpha d_{xy}+\tfrac{1}{2}\beta(s_1-s_2-s_3+s_4)+\tfrac{1}{2}\gamma(\sigma_1-\sigma_2-\sigma_3+\sigma_4)+\tfrac{1}{4}\delta[(-\pi_{1x}+\pi_{2x}+\pi_{3x}-\pi_{4x})+3^{1/2}(\pi_{1y}-\pi_{2y}-\pi_{3y}+\pi_{4y})]\ ,$$

$$\Psi_{yz}=\alpha d_{yz}+\tfrac{1}{2}\beta(s_1-s_2+s_3-s_4)+\tfrac{1}{2}\gamma(\sigma_1-\sigma_2+\sigma_3-\sigma_4)+\tfrac{1}{4}\delta[(-\pi_{1x}+\pi_{2x}-\pi_{3x}+\pi_{4x})-3^{1/2}(\pi_{1y}-\pi_{2y}+\pi_{3y}-\pi_{4y})]\ , \tag{2}$$

$$\Psi_{zx}=\alpha d_{zx}+\tfrac{1}{2}\beta(s_1+s_2-s_3-s_4)+\tfrac{1}{2}\gamma(\sigma_1+\sigma_2-\sigma_3-\sigma_4)+\tfrac{1}{2}\delta[(\pi_{1x}+\pi_{2x}-\pi_{3x}-\pi_{4x})]\ .$$

The numbers 1, 2, 3, and 4 refer to the four carbons at the positions 111, $\bar{1}1\bar{1}$, $1\bar{1}\bar{1}$, and $\bar{1}\bar{1}1$, respectively. The orbitals designated by σ are $2p$ orbitals of the carbons which have lobes pointing towards the central nickel ion, while the orbitals designated by π are $2p$ orbitals with lobes perpendicular to the carbon-nickel bond axis. The value of $\beta^2+\gamma^2+\delta^2$ gives the sum of the spin densities on the four nearest-neighbor carbons. For d^7 ($e^4t_2^3$) configuration, the ground state is an orbital singlet and it is possible to sum the separate contributions to the hyperfine interaction from the individual, singly occupied orbitals.[29] We obtain the ^{13}C superhyperfine tensor of the nearest neighbors as

$$A_{\parallel}=A_s+2(A_d+A_\sigma-A_\pi)\ ,$$
$$A_{\perp}=A_s-(A_d+A_\sigma-A_\pi)\ , \tag{3}$$

with

$$A_s=1/(2S)\tfrac{3}{4}\beta^2g\mu_Ba_0\ ,$$
$$A_d=1/(2S)3\alpha^2g\mu_Bb_{dd}\ ,$$
$$A_\sigma=1/(2S)\tfrac{3}{4}\gamma^2g\mu_Bb_0\ ,$$
$$A_\pi=1/(2S)\tfrac{3}{8}\delta^2g\mu_Bb_0\ ,$$
$$a_0=\tfrac{2}{3}\mu_0g_n\mu_n|\Psi(0)|_{2s}^2\ ,$$
$$b_0=\tfrac{2}{5}\mu_0/(4\pi)g_n\mu_n\langle r^{-3}\rangle_{2p}\ ,$$
$$b_{dd}=\mu_0/(4\pi)g_n\mu_nR^{-3}\ ,$$

where the total spin $S=\frac{3}{2}$, $\Psi(0)$ is the wave function at the nucleus, and r is the electron-nuclear separation distance.

The unpaired electron localized 100% in a carbon $2s$ orbital produces an isotropic hyperfine interaction $a_0=111.9$ mT and in a carbon $2p$ orbital an anisotropic

hyperfine interaction $b_0=3.19$ mT.[30] The isotropic part A_s is the contribution from the 2s orbital. From the observed value of the isotropic part (0.673 mT), β^2 is estimated to be 0.0237. Among the contributions to the anisotropic part, A_d is the dipolar interaction between the magnetic moment of the electrons on the central nickel ion and the magnetic moment of the ^{13}C nucleus. Assuming $\alpha^2=1$, with 100% spin localization on the central nickel ion and taking the Ni—^{13}C bond distance $R=1.54$ Å, A_d is estimated to be 0.197 mT using the point dipole approximation. From the observed value of the anisotropic part (0.333 mT), $A_\sigma - A_\pi$ is 0.136 mT. The hyperfine interactions with carbon 2p orbitals A_σ and A_π cannot be separated experimentally. As the contributions from the σ and π orbitals counteract each other, only the minimum value of the spin density on carbon 2p orbitals can be estimated. Taking $\delta^2=0$, γ^2 is estimated to be 0.168. If we constrain $\alpha^2+\beta^2+\gamma^2+\delta^2=1$ instead of taking $\alpha^2=1$, we obtain $\alpha^2=0.746$, $\beta^2=0.0237$, $\gamma^2=0.230$ with $\delta^2=0$. Thus spin delocalization of at least 25% onto the nearest-neighbor carbons is estimated. If we allow some structural relaxation to increase the Ni—^{13}C bond distance to $R=1.60$ Å, we obtain $\alpha^2=0.721$, $\beta^2=0.0237$, $\gamma^2=0.255$ with $\delta^2=0$.

The LCAO treatment can be extended to the spin delocalization on the twelve next-nearest-neighbor carbons. The deviation from axial symmetry of the ^{13}C superhyperfine tensor is small and will be ignored. From the observed value of the isotropic part (0.308 mT), the total spin density on the 2s orbital of the next-nearest neighbors is estimated to be 0.033. The LCAO describing the delocalization onto the next-nearest neighbors contain several parameters for the admixture of σ and π orbitals.[28] These parameters cannot be separated experimentally. The total spin density on the 2p orbital of the next-nearest neighbors depends strongly on the assumptions used in their estimation. We will denote the principal axis associated with the largest absolute principal value as the unique axis. Among the twelve next-nearest-neighbor carbons, two carbons are located in a $(\bar{1}10)$ plane through the central ion. These two carbons are on a [110] axis through the central ion. In one carbon, bonded to the nearest-neighbor carbon in the [111] direction relative to the central ion, the C—C bond to the nearest neighbor is parallel to the $[\bar{1}\bar{1}1]$ axis. In the other carbon, bonded to the nearest-neighbor carbon of the $[\bar{1}\bar{1}1]$ direction, the C—C bond to the nearest-neighbor carbon is parallel to the [111] axis. As shown in Fig. 6, the unique axis appears 60° from the [001] axis and 120° from the [001] axis in the $(\bar{1}10)$ plane. We note that the unique axis is nearly ($\sim$5°) parallel to either the [111] axis or the $[\bar{1}\bar{1}1]$ axis. The superhyperfine tensor with the unique axis nearly parallel to the $[\bar{1}\bar{1}1]$ axis is assignable to either one of the two carbons above. From both assignments, the rotation pattern of the angular dependence shown in Fig. 6 is generated by the symmetry operation and no unique assignment can be made. The contribution to the anisotropic part of the dipolar interaction between the spin density on the central nickel ion and the ^{13}C nucleus of the next-nearest neighbor is estimated to be $A_d=0.0337$ mT for a distance $R=2.52$ Å and spin localization on the nickel of $\alpha^2=0.75$. The magnitude of the anisotropic part observed (0.037 mT) is comparable to this estimation. If we take 0.003 mT (0.037 − 0.0337 mT) arising from the admixture of the 2p orbitals of the next-nearest neighbors, the total spin density on the 2p orbitals of the next-nearest neighbors is estimated to be 0.01. However, the unique axis observed is 30° away from the [110] axis which is the direction connecting the central ion and the next-nearest-neighbor carbon. Thus the anisotropic part is not dominated by the dipolar interaction between the spin density on the central ion and the ^{13}C nucleus and/or by the spin transfer to the 2p orbitals involved in metal-carbon σ bonding. The deviation of the unique axis from the [110] axis might be caused by admixture of the 2p orbitals in the metal-carbon π bonds.

Another estimate can be obtained assuming that the anisotropic part of the hyperfine interaction is dominated by two contributions: (1) spin density in the 2p orbital of the next-nearest-neighbor carbon with lobes pointing toward the nearest neighbor and (2) the dipolar interaction between the spin density on the nearest neighbor and the ^{13}C nucleus. Using 25% delocalization to the nearest neighbors, the dipolar interaction between spin density on the nearest neighbors and the ^{13}C nucleus of the next-nearest neighbors is estimated to be 0.012 mT with $R=1.54$ Å. Taking 0.025 mT (0.037 − 0.012 mT) as arising from the admixture of the 2p orbital of the next-nearest neighbor, the total spin density on the 2p orbital of the next-nearest neighbors is estimated to be 0.093. Thus spin delocalization onto the next-nearest neighbors is estimated to be between 4% and 13% depending on the assumptions used. Unless the spin densities on the next-nearest neighbors are negligibly small, normalization of the wave function so that the sum of the unpaired spin densities becomes unity is required. Because of the ambiguity in estimating the next-nearest-neighbor spin density, we do not attempt the normalization here.

E. Charge compensation

Our assignment of the charge of Ni^- leaves the problem of the charge-compensation mechanism. A charged species in diamond must be compensated by another charged species in order to maintain charge neutrality of the lattice. In silicon, the desired charge state of the transition metal is obtained by adjusting the Fermi level with the proper concentration of shallow donors or shallow acceptors. Because the crystals used in this study are nonsemiconducting diamond, the extra electron on the Ni could not be supplied from the conduction electrons. The donor electron of the N impurity is bound so it could not provide charge compensation. The high symmetry of the EPR spectrum of the Ni as well as the ^{13}C hyperfine with surrounding carbons indicates that there is no nearby, charge-compensating impurity or defect. However, a more distant charge-compensating ion could provide a ready mechanism for the weak distortion of the center that seems to occur at low temperatures.

Our experiments appear to completely rule out the model that the $g=2.0319$ EPR spectrum is a carbon-

centered defect.[31] It is difficult to envision a carbon-centered, substitutional defect with tetrahedral local symmetry. In addition, cw-EPR spectra on sample B (10% ^{13}C) showed no ^{13}C hyperfine splitting from a central carbon atom.

IV. CONCLUSION

The $g=2.0319$ EPR signal in synthetic diamonds arises from a substitutional Ni^- ($3d^7$) with effective spin $S=\frac{3}{2}$. It is curious that Ni seems to be the only transition metal incorporated as a dispersed species into synthetic diamonds even though many other transition metals are used as solvents. Although we have characterized this Ni defect, the existence of other Ni defects or other transition-metal defects is by no means excluded. Transition metals can certainly be incorporated as inclusions; dispersed, nonparamagnetic defects; or unobserved paramagnetic defects. Integral-spin species at low-symmetry sites could well have fine-structure splittings too large to be observed at the typical 9-GHz EPR frequency. Species with efficient spin-lattice relaxation mechanisms may be extremely broadened and undetectable except at very low temperatures. Other transition-metal impurity species may yet be found by EPR in synthetic diamond by searching at low temperatures, by varying the Fermi level through doping, by irradiation, and by growing crystals in new metal solvents or under different conditions.

ACKNOWLEDGMENTS

This work was supported in part by the Office of Basic Energy Sciences, Division of Chemical Sciences, U.S. Department of Energy, under Contract No. W-31-109-Eng-38. Several crystals used in the initial stages of this work were supplied by Itami Laboratory,, Sumitomo Electric Industries.

[1]R. C. Burns, in Proceedings of the First International Conference on the New Diamond Science and Technology, Tokyo, 1988 (in press).

[2]G. W. Ludwig and H. H. Woodbury, in *Solid State Physics,* edited by F. Seitz and D. Turnbull (Academic, New York, 1962), Vol. 13, p. 223.

[3]R. van Kemp, E. G. Sieverts, and C. A. J. Ammerlaan, Phys. Rev. B **36**, 3528 (1987).

[4]J. H. N. Loubser and W. P. van Ryneveld, Nature (London) **211**, 517 (1966).

[5]M. I. Samoilovich, G. N. Bezrukov, and V. P. Butuzov, Pis'ma Zh. Eksp. Teor. Fiz. **14**, 551 (1971) [JETP Lett. **14**, 379 (1971)].

[6]G. W. Ludwig and H. H. Woodbury, Phys. Rev. **113**, 1014 (1959).

[7]R. H. Wentorf, Jr., J. Phys. Chem. **75**, 1833 (1971).

[8]H. M. Strong and M. H. Chrenko, J. Phys. Chem. **75**, 1838 (1971).

[9]J. R. Norris, M. C. Thurnauer, and M. K. Bowman, in *Advances in Biological and Medical Physics,* edited by J. H. Lawrence, T. W. Gofman, and T. L. Hayes (Academic, New York, 1980), Vol. 17, pp. 365–415.

[10]R. J. Massoth, Ph.D. dissertation, University of Kansas, 1987.

[11]A. Angerhofer, R. J. Massoth, and M. K. Bowman, Isr. J. Chem. **28**, 227 (1988).

[12]W. V. Smith, P. P. Sorokin, I. L. Gelles, and G. J. Lasher, Phys. Rev. **115**, 1546 (1959).

[13]J. Isoya, C. P. Lin, M. K. Bowman, J. R. Norris, S. Yazu, and S. Sato, in Proceedings of the First International Conference on the New Diamond Science and Technology, Tokyo, 1988 (in press).

[14]G. W. Ludwig, Phys. Rev. **137**, A1520 (1965).

[15]K. L. Brower, Phys. Rev. B **1**, 1908 (1970).

[16]J. Isoya, M. K. Bowman, J. R. Norris, and J. A. Weil, J. Chem. Phys. **78**, 1735 (1983).

[17]M. K. Bowman and R. J. Massoth, in *Electronic Magnetic Resonance of the Solid State,* edited by J. A. Weil, M. K. Bowman, J. R. Morton, and K. F. Preston (Canadian Society for Chemistry, Ottawa, 1987), pp. 99–110.

[18]W. B. Mims, in *Electron Paramagnetic Resonance,* edited by S. Geschwind (Plenum, New York, 1972), pp. 263–351.

[19]K. M. Salikhov, A. G. Semenov, and Yu. D. Tsvetkov, *Electron Spin Echoes and Their Applications* (Nauk, Novosibirsk, 1976).

[20]L. Kevan, in *Time Domain Electron Spin Resonance,* edited by L. Kevan and R. N. Schwartz (Wiley, New York, 1979), pp. 279–342.

[21]J. Tang and J. R. Norris, J. Magn. Reson. **79**, 190 (1988).

[22]F. M. M. Geurts, A. P. M. Kentgens, and W. S. Veeman, Chem. Phys. Lett. **120**, 206 (1985).

[23]A. P. M. Kentgens, J. J. M. Lemmens, F. M. M. Geurts, and W. S. Veeman, J. Magn. Reson. **71**, 62 (1987).

[24]A. Abragam, *Principles of Nuclear Magnetism* (Oxford University Press, Oxford, 1961).

[25]J. R. Klauder and P. W. Anderson, Phys. Rev. **125**, 912 (1962).

[26]I. M. Brown, in *Time Domain Electron Spin Resonance,* edited by L. Kevan and R. N. Schwartz (Wiley, New York, 1979), pp. 195–229.

[27]F. S. Ham, G. W. Ludwig, G. D. Watkins, and H. H. Woodbury, Phys. Rev. Lett. **5**, 468 (1960).

[28]D. A. van Wezep, R. van Kemp, E. G. Sieverts, and C. A. J. Ammerlaan, Phys. Rev. B **32**, 7129 (1985).

[29]J. Owen and J. H. M. Thornley, Rep. Prog. Phys. **29**, 675 (1966).

[30]B. A. Goodman and J. B. Raynor, in *Advances in Inorganic Chemistry and Radiochemistry,* edited by H. J. Emeleus and A. G. Sharpe (Academic, New York, 1970), Vol. 13, pp. 135–362.

[31]Yu. A. Bratashevskii, F. N. Bukhan'ko, N. D. Samsonenko, and O. Z. Shapiro, Fiz. Tverd. Tela. (Leningrad) **13**, 2154 (1971) [Sov. Phys.—Solid State **13**, 1809 (1972)].